Vol. 13, pp. 227–233 (2016)
doi: 10.2142/biophysico.13.0_227

Biophysics and Physicobiology
https://www.jstage.jst.go.jp/browse/biophysico/

Regular Article

Domain-based biophysical characterization of the structural and thermal stability of FliG, an essential rotor component of the Na^+-driven flagellar motor

Yasuhiro Onoue[1], Rei Abe-Yoshizumi[†1], Mizuki Gohara[1], Yuuki Nishino[1], Shiori Kobayashi[1], Yasuo Asami[2] and Michio Homma[1]

[1]*Division of Biological Science, Graduate School of Science, Nagoya University, Nagoya, Aichi 464-8602, Japan*
[2]*TA Instruments Japan Inc., Gotanda, Shinagawa-ku, Tokyo 141-0031, Japan*

Received March 28, 2016; accepted August 22, 2016

Many bacteria move using their flagellar motor, which generates torque through the interaction between the stator and rotor. The most important component of the rotor for torque generation is FliG. FliG consists of three domains: $FliG_N$, $FliG_M$, and $FliG_C$. $FliG_C$ contains a site(s) that interacts with the stator. In this study, we examined the physical properties of three FliG constructs, $FliG_{Full}$, $FliG_{MC}$, and $FliG_C$, derived from sodium-driven polar flagella of marine *Vibrio*. Size exclusion chromatography revealed that FliG changes conformational states under two different pH conditions. Circular dichroism spectroscopy also revealed that the contents of α-helices in FliG slightly changed under these pH conditions. Furthermore, we examined the thermal stability of the FliG constructs using differential scanning calorimetry. Based on the results, we speculate that each domain of FliG denatures independently. This study provides basic information on the biophysical characteristics of FliG, a component of the flagellar motor.

Key words: DSC, FliG, rotor, flagellar motor

The flagellum is an organelle for locomotion and is composed of a filament, hook, and basal body. The basal body, which contains the rotor, comprises several ring structures, the L, P, MS, and C rings. The stator, which is an ion-conducting energy-converting complex, surrounds the rotor and generates torque through interaction with components of the rotor [1,2]. The flagellar motor uses mainly two kinds of ions, H^+ or Na^+, as the energy source and the stator is composed of two kinds of membrane proteins. *Escherichia coli* and *Salmonella enterica* have proton driven motors and the stator is composed of the MotA and MotB proteins. On the other hand, *Vibrio* has Na^+ driven motors and the stator is composed of the proteins PomA and PomB [3,4]. MotA and

Abbreviations: PomA, Polar flagellar motility protein A; PomB, Polar flagellar motility protein B; SDS-PAGE, sodium dodecyl sulfate-polyacrylamide gel electrophoresis; CD, circular dichroism

Corresponding author: Michio Homma, Division of Biological Science, Graduate School of Science, Nagoya University, Furo-cho, Chikusa-ku, Nagoya, Aichi 464-8602, Japan.
e-mail: g44416a@cc.nagoya-u.ac.jp
[†]Present address: Department of Frontier Materials, Nagoya Institute of Technology, Nagoya, Japan.

◀ ***Significance*** ▶

Bacteria can swim by rotating their flagella. Interaction between the stator protein and the rotor protein makes the rotational driving force. FliG is the most important component of the rotor for the torque generation in the flagellar motor. Here, we purified FliG and its fragmants from *Vibrio alginolyticus*, which has a polar flagellum to characterize the biochemical/biophysical properties by gel-filtration chromatography, circular dichroism spectroscopy, and differential scanning calorimetry. The results suggest that FliG has at least two conformational states and that each domain of FliG is responsible for the denaturation. These provide information on the basic characteristics of FliG.

PomA have four transmembrane regions, whereas MotB and PomB have only one. MotA and MotB, and PomA and PomB form a complex with a stoichiometry of A4:B2 [5,6]. It has been suggested that MotB and PomB undergo a dynamic conformational change in order to bind to the peptidoglycan layer [7,8].

To reach a favorable condition, bacteria have a chemotactic system to regulate the rotational direction of the flagellar motor. In the flagellar motor, the C ring plays a role in the directional change, counterclockwise (CCW) and clockwise (CW), thus it is also called the switch complex. In *E. coli*, which has peritrichous flagella, the CCW rotation of the flagella leads to the forward pushing of the bacterial cell body, leading to a smooth swimming motion. On the other hand, the CW rotation leads to the unwinding of the flagellar filament bundle and the bacteria tumble [9]. The C ring is composed of three proteins, FliG, FliM, and FliN, which are cytoplasmic, not transmembrane proteins [10]. FliM is divided into three domains, $FliM_N$, $FliM_M$, and $FliM_C$. FliG is also divided into three domains, $FliG_N$, $FliG_M$, and $FliG_C$. $FliG_N$ interacts with FliF, which is the MS ring component. $FliG_M$ and $FliG_C$ interact with FliM [11,12]. $FliM_N$ interacts with CheY-P, the phosphorylated form of CheY, which is a response regulator [13,14]. When CheY-P binds $FliM_N$, the flagella rotate CW. If the concentration of CheY-P decreases, the flagella rotate CCW. The crystal structures of the C ring component proteins, FliG, FliM, and FliN, have been revealed. The structural difference of FliG between the CW and the CCW state has been proposed from the crystal structures of FliG [15–19]. Recently, in the C ring structure it was shown for the $FliM_M$:$FliG_M$ heterodimer and it was also detected that higher-order assemblies include a parallel back-to-front arrangement of the $FliM_M$ units [20]. Furthermore, NMR analysis has been reported for *Thermotoga maritima* [12,21], and the HSQC spectra obtained revealed the interaction between FliF or FliM and FliG.

The most important rotor component for torque generation is FliG, which interacts with the stator protein, PomA or MotA [22]. It has been shown that the electrostatic interactions between some conserved charged residues of the cytoplasmic loop of MotA ($MotA_{loop}$) and the C-terminal domain of FliG ($FliG_C$) are important for torque generation of the H^+-driven flagellar motor of *E. coli* [1]. On the other hand, the Na^+-driven flagellar motor of marine *Vibrio* contains such conserved charged residues in PomA and FliG, but single mutations of these conserved residues do not strongly affect the motility [23,24]. Compared with *E. coli*, the number of conserved charged residues of the flagellar motor in *Vibrio* is greater, and the contribution of each residue for torque generation may be smaller in *Vibrio* motor [2,25]. Furthermore, we found that a specific interaction between the charged residues is critical for the correct assembly of the stators around the rotor and is important for torque generation [2].

It has been reported that there are other important residues or motifs of FliG for motility in addition to the charged residues. For example, in *E. coli* and *Helicobacter pylori*, the motif of $FliG_C$ containing the MFXF sequence is thought to be important for the motor switch [19]. In *Vibrio alginolyticus*, the three-residue deletion mutant, ΔPSA, which corresponds to ΔPEV in *T. maritima,* showed loss of motility [26]. In addition to this mutant, three other Mot^- mutants, L259Q, L270R, and L271P of FliG, were reported in *V. alginolyticus* [27]. We have characterized the physical properties of the C-terminal domain (G214–L351) of wild-type FliG and its non-motile phenotype mutant derivatives [28]. The CD spectra and size exclusion chromatography did not show a significant difference between the wild-type and mutant FliG proteins, however, the DSC data were very different between the mutants. This possibly means that the secondary structure is not affected by the mutation but the tertiary structure is.

In this study, we made new constructs of plasmids containing the *fliG* gene and overexpressed FliG of marine *Vibrio*, $FliG_{MC}$, and full length FliG in addition to the C-terminal domain of FliG ($FliG_C$). We then characterized the physical properties of FliG using these truncated *Vibrio* FliG proteins.

Materials and Methods

Strains and plasmids

The strains and plasmids used in this study are shown in Table 1. Routine DNA manipulations were carried out according to standard procedures using the *E. coli* strain DH5α. *E. coli* strain BL21 was used for protein expression.

Protein expression in *E. coli* and purification

The expression plasmids were introduced into *E. coli* strain BL21. Cells were grown and induced as described previously [28]. Cells were harvested by centrifugation, suspended in TN buffer [50 mM Tris-HCl (pH 8.0), 0.5 M NaCl] containing 20 mM imidazole and protease inhibitors, and were disrupted by sonication (LV 5.0, duty cycle 50%, 1 min×5). After the suspension was centrifuged at 22,000×*g* for 15 min, the supernatant was ultracentrifuged at 100,000×*g* for 30 min. The supernatant of the soluble fraction was subjected to

Table 1 Strains and plasmids used in this study

Strain or plasmid	Description	Source or reference
Escherichia coli		
BL21	Host for overexpression from the T7 promoter	
DH5a	Recipient for cloning experiments	
Plasmid		
pColdI	Cold shock expression vector	Takara
pCold-$FliG_C$	pColdI/FliG (G214–L351)	[28]
pCold-$FliG_{MC}$	pColdI/FliG (G122–L351)	This study
pRAY201	pColdI/FliG (Full)	[31]

affinity column chromatography using the His Trap HP 5 ml (Ni-NTA) column (GE Healthcare). Proteins were eluted with an imidazole concentration gradient (from 20 mM to 500 mM) and collected by 1 ml fraction. The collected fractions were subjected to SDS-PAGE and Coomassie brilliant blue (CBB) staining to examine the purity of the proteins.

SDS-PAGE

Samples for SDS-PAGE were mixed with the SDS sample buffer and boiled at 95°C for 10 min. SDS-PAGE was performed using a 12% polyacrylamide gel.

Size exclusion chromatography

The sample was subjected to the gel filtration column using a Superdex 200 10/300 (GE healthcare). Size exclusion chromatography was performed using either 50 mM sodium phosphate (pH 6.5) or 50 mM Tris-HCl (pH 8.0) buffer at a flow rate of 0.5 ml/min, and samples were fractionated by 1 ml. The molecular weight was estimated using the marker proteins, ribonuclease A, carbonic anhydorase, ovalbumin, conalbumin, aldolase, ferritin, and thyroglobulin (GE healthcare).

Circular dichroism spectroscopy

Circular dichroism spectroscopy was measured using a J-720W instrument (Jasco) as described previously [28]. All sample concentrations were 0.1 mg/ml and buffer conditions were 50 mM sodium phosphate (pH 6.5 or pH 8.0). The spectra obtained were analyzed using Secondary structure prediction program (JASCO). The Yang equation was used as a reference to obtain the secondary structure ratio.

Differential scanning calorimetry (DSC)

The purified FliG constructs were inserted using a syringe into a Slide-A-Lyzer (PIERCE) and dialyzed against a 50 mM phosphate buffer (pH 6.5). The dialyzing buffer was replaced after 3 hours and further dialyzed overnight at 4°C. The dialyzed sample (650 µl of 1 mg/ml sample) was applied into a nano-DSC differential scanning calorimeter (TA Instruments) and the heat capacity and thermal stability were measured with a scan speed of 1°C/min from 15 to 90°C against the reference buffer of 50 mM phosphate (pH 6.5).

Results

Purification profiles of FliG

Recently we reported on the biophysical characteristics of the FliG C-terminal domain, $FliG_C$, from *V. alginolyticus* [28]. Using the same analytical techniques, we characterized two other constructs, FliG full length ($FliG_{Full}$), and FliG middle and C-terminal domain ($FliG_{MC}$), in addition to $FliG_C$ (Fig. 1). We expressed these constructs in *E. coli* and purified them. As shown in the SDS-PAGE CBB staining results in Figure 2A, all constructs were expressed well and were purified as a single band. However, the expression levels of

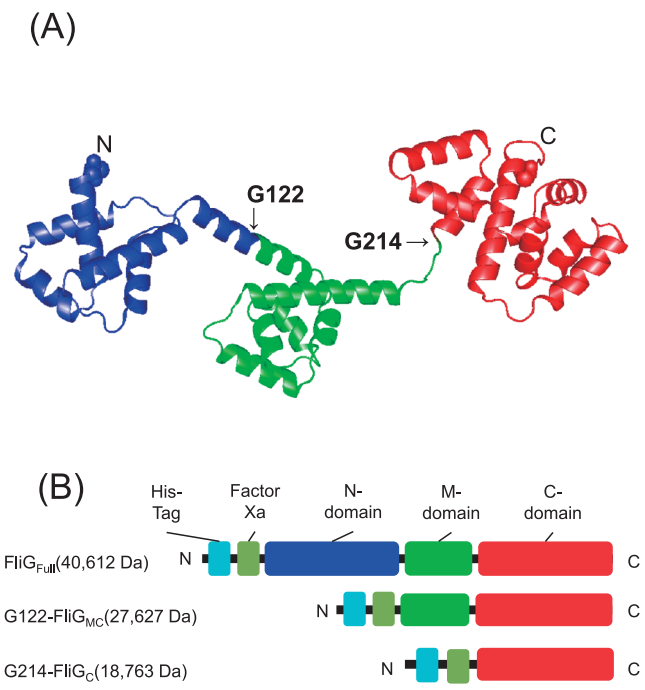

Figure 1 (A): The crystal structure of full length FliG in *Aquifex aeolicus*. The N-terminal domain, middle domain, and C-terminal domain are colored blue, green, and red, respectively. G122 corresponds to the predicted N-terminal residue of FliG middle domain in *Vibrio alginolyticus*. G214 corresponds to the predicted N-terminal residue of FliG C-terminal domain in *V. alginolyticus*. (B): The three constructs of FliG used in this study. G122-$FliG_{MC}$ corresponds to the middle and C-terminal domains and G214-$FliG_C$ corresponds to the same C-terminal domain as (A).

$FliG_{Full}$ and $FliG_{MC}$ were higher than that of $FliG_C$. Additional bands were detected in purified $FliG_C$, suggesting that $FliG_C$ is digested during the purification step. $FliG_C$ seems to be more unstable than $FliG_{Full}$ and $FliG_{MC}$.

Size exclusion chromatography of FliG

We analyzed all the FliG constructs using size exclusion chromatography under two conditions: 50 mM Tris-HCl (pH 8.0) buffer and 50 mM sodium phosphate buffer (pH 6.5) (Fig. 2B, C). Under both conditions, all constructs were eluted as a single peak, but the peak position was dependent on the buffer condition. In the Tris-HCl buffer at pH 8.0, the estimated molecular weights of $FliG_{Full}$, $FliG_{MC}$, and $FliG_C$ were ca. 155 kDa, ca. 87 kDa, and ca. 50 kDa, respectively. In the sodium phosphate buffer at pH 6.5, the estimated molecular weights of $FliG_{Full}$, $FliG_{MC}$, and $FliG_C$ were ca. 58 kDa, ca. 53 kDa, and ca. 24 kDa, respectively. The estimated molecular weights under conditions of higher pH seem to be higher than those under lower pH. In particular, the estimated molecular weight of $FliG_{Full}$ was dramatically different between the two conditions. These results suggest that the conformation of FliG, especially that of $FliG_{Full}$, was changed between the two buffer conditions.

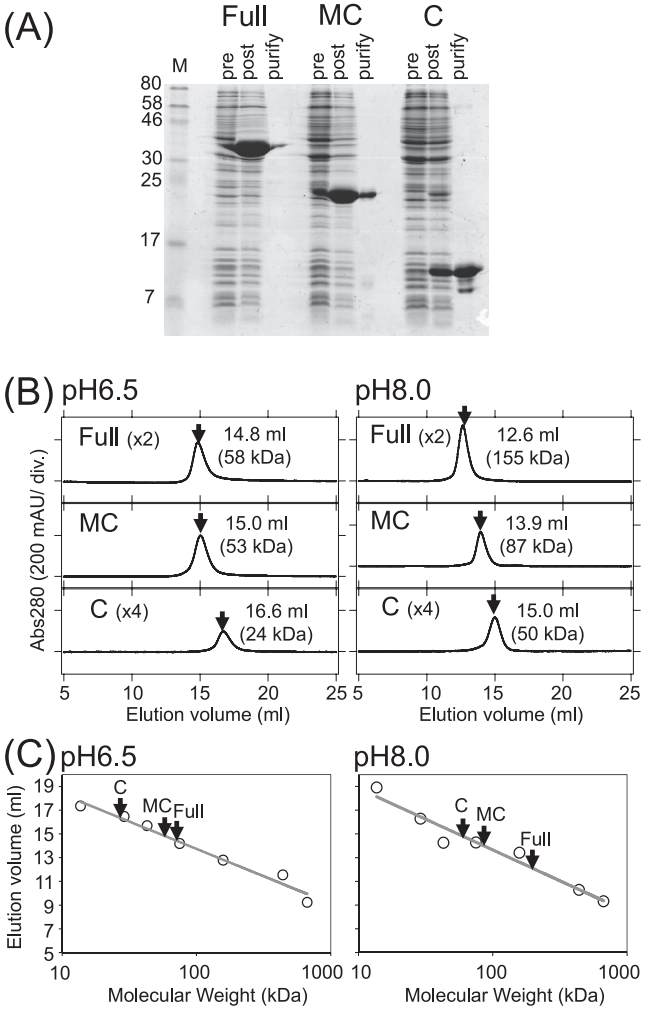

Figure 2 Purification profiles of FliG constructs. (A): CBB staining results. Pre indicates pre induction whole cell sample, post indicates post induction whole cell sample, and purify indicates the purification product sample. M: molecular weight markers. (B): The profiles of size exclusion chromatography. The arrows show the peaks derived from the purification product. The elution volume (ml) of the peak and the estimated molecular weight (kDa) are shown in each profile. Left, results under 50 mM sodium phosphate buffer at pH 6.5. Right, results under 50 mM Tris-HCl buffer at pH 8.0. Full: full length $FliG_{Full}$, MC: $FliG_{MC}$ and C: $FliG_{C}$. x2 and x4 in brackets mean the multiplication of the vertical scales. (C): Calibration curves at pH 6.5 and at pH 8.0 were drawn using the molecular weight markers.

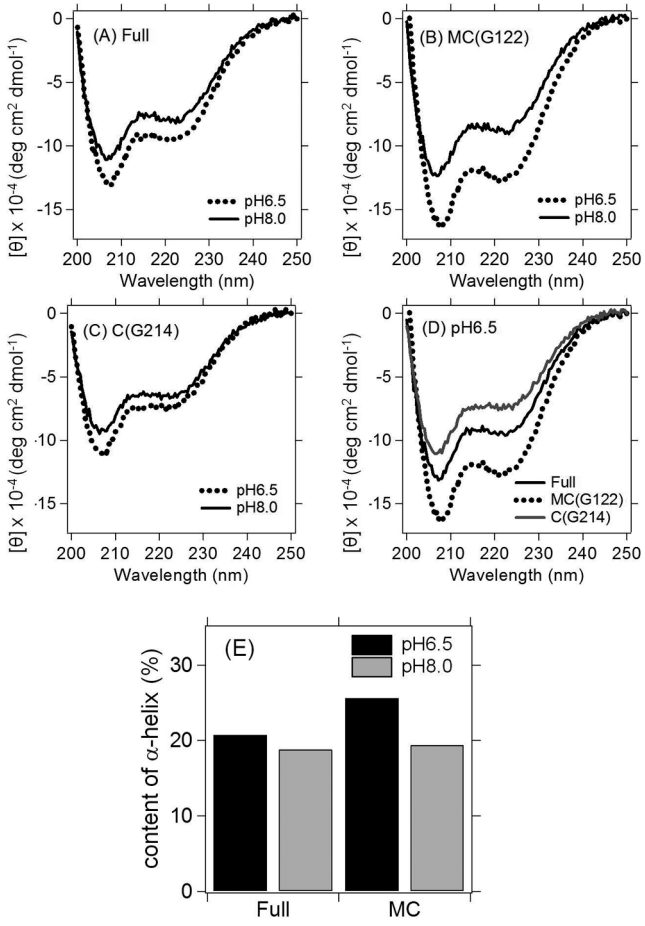

Figure 3 CD spectra of FliG constructs. (A), (B), and (C): The CD spectra data comparing pH 6.5 to pH 8.0. Solid lines show the results at pH 6.5 and dotted lines show the results at pH 8.0. (A): full length FliG; $FliG_{Full}$, (B): middle and C-terminal domain construct of FliG; $FliG_{MC}$ and (C): C-terminal domain construct of FliG; $FliG_{C}$, respectively. (D): Data comparing CD spectra of all constructs at pH 6.5. Solid line: $FliG_{Full}$; dotted line: $FliG_{MC}$; and gray line: $FliG_{C}$. All sample concentrations were 0.1 mg/ml and buffer conditions were 50 mM sodium phosphate buffer pH 6.5 or pH 8.0. (E): The structural compositions are estimated using software from JASCO and the percentages of the structures for α-helix are indicated.

Circular dichroism spectroscopy of FliG

The results of size exclusion chromatography suggest that the conformation of all FliG constructs changes depending on the buffer conditions. Next, we tried detecting the possibility of secondary structural changes of FliG using circular dichroism (CD) spectroscopy (Fig. 3). The CD spectra of all FliG constructs under both pH conditions show the negative peak around 207 nm and the negative shoulder around 222 nm (Fig. 3). These spectra are typical of α-helical conformation, which is supported by the fact that the crystal structures of FliG from various species are mainly composed of α-helices (Fig. 1). Comparing the spectra at pH 6.5 with those at pH 8.0, the negative peak and shoulder at pH 6.5 are deeper than those at pH 8.0 for all FliG constructs. Therefore, this shows that the structures of FliG at pH 6.5 have more α-helices than those at pH 8.0. Comparing the spectra among the FliG constructs, the spectra of $FliG_{MC}$ show the most negative peak and shoulder under both pH conditions (Fig. 3D). Moreover, $FliG_{Full}$ showed a more negative peak and shoulder than $FliG_{C}$. We estimated the content of α-helices in $FliG_{Full}$ and $FliG_{MC}$. There was little difference under both pH conditions and the contents at pH 6.5 were higher than those at pH 8.5 (Fig. 3E).

Differential scanning calorimetry of FliG

We used differential scanning calorimetry (DSC) to investigate the thermal stability of the FliG constructs (Fig. 4). We measured the FliG constructs at pH 6.5, in which they showed more negative molar ellipticities. $FliG_C$ showed a clear single peak, suggesting that the thermal denaturation of $FliG_C$ is a one-step process. Fitting this peak by a two state model, the T_m value is ca. 59°C and the corrected Van't Hoff enthalpy, ΔH, is 208 kJ/mol, which are similar to our previous report [28]. In contrast, the DSC curves of $FliG_{MC}$ and $FliG_{Full}$ can be fitted with two and three peaks, respectively. The T_m values are ca. 42°C and ca. 60°C, and the estimated ΔH values are 197 kJ/mol and 95 kJ/mol for the first and second peaks of $FliG_{MC}$, respectively. The T_m values are ca. 53°C, ca. 59°C, and ca. 67°C, and the estimated ΔH values are 85 kJ/mol, 162 kJ/mol, and 53 kJ/mol for the first, second, and third peaks of $FliG_{Full}$, respectively. Importantly, the number of peaks is consistent with the number of domains in the FliG constructs. Therefore, our results imply that each domain of FliG thermally denatures independently and the thermal stability is affected by the interaction of the other domain or the linker between domains.

Discussion

In this study, we investigated the biophysical characteristics of FliG by comparing $FliG_{Full}$ with its fragments, $FliG_{MC}$ and $FliG_C$. The results of size exclusion chromatography imply the conformational change of FliG between the two pH conditions (Fig. 2B, C). The estimated molecular weight of the constructs by size exclusion chromatography was larger than that calculated using their amino acid sequences. We cannot conclude whether this might be due to the formation of higher order complexes (dimer or trimer) or not. A recent study found that the conformation of FliG can be changed between an extended and compact form depending on the NaCl concentration [29]. Furthermore, it has been demonstrated that FliG exists as a monomer in solution but as a domain-swapped polymer in the flagellar motor [29].

$FliG_{Full}$ showed the largest change in the apparent molecular weight between pH 6.5 and 8.0 among the constructs (Fig. 2). This implies that $FliG_{Full}$ at pH 8.0 exists primarily in an extended form compared with that at pH 6.5, where it exists primarily in a compact form. $FliG_{MC}$ and $FliG_C$ showed similar profiles at both pH 6.5 and pH 8.0. The theoretical pIs of $FliG_{Full}$, $FliG_{MC}$, and $FliG_C$ are 4.5, 4.4, and 4.3, respectively. Thus, we propose that the electrostatic interactions contribute to the pH dependent conformational changes in FliG. Simply speaking, there are more electrostatic charges under pH 8.0 since it is farther from the theoretical pIs of the constructs than pH 6.5, promoting FliG to form its extended conformation. This is consistent with the recent study that found that FliG exists in its extended form under lower NaCl concentrations but under higher NaCl concentrations in its compact form [29]. Usually, the high concentration of salt

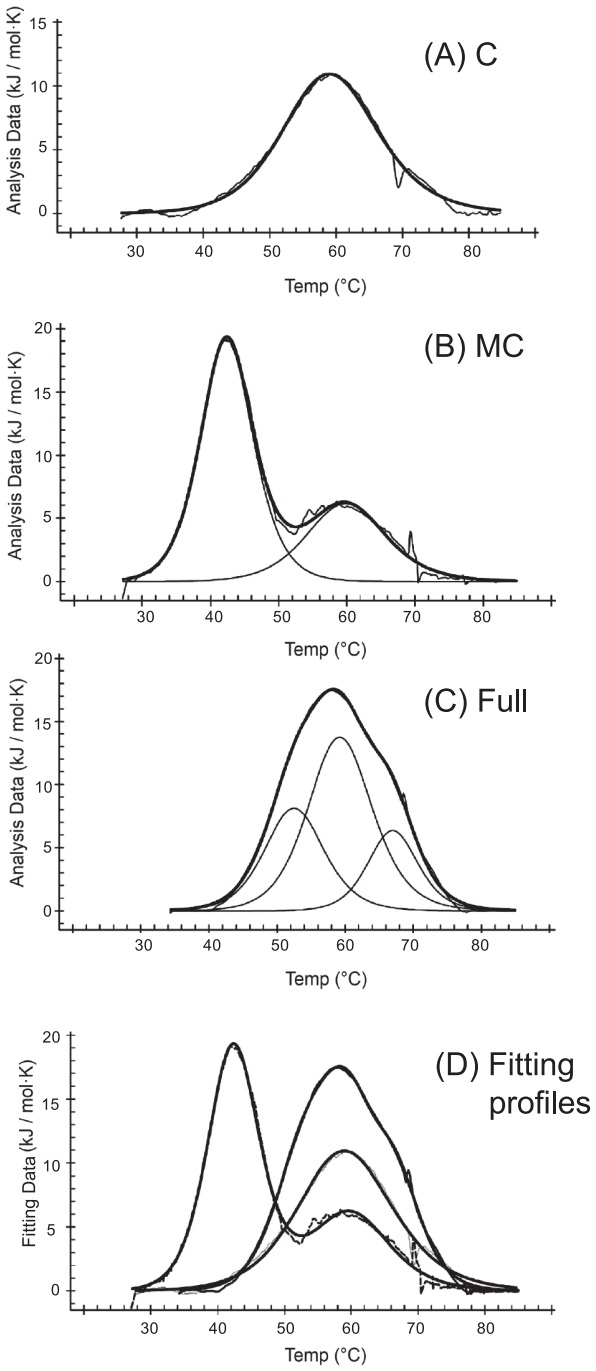

Figure 4 DSC data of FliG constructs under 50 mM sodium phosphate buffer at pH 6.5. The scan range was 15 to 90°C and the scan rate was 1 degree/min. The vertical and horizontal axes show molar heat capacity and temperature, respectively. (A) The profiles of G214-$FliG_C$: C. The thin line and the solid line show the raw data and the results fitted by the two state scaled model, respectively. (B) The profiles of G122-$FliG_{MC}$: MC. The smooth lines show the results fitted by the two state scaled model. The solid line shows the result of the model sum. The line shows raw data. (C) The profiles of full length $FliG_{Full}$: Full. The thin smooth lines show the results fitted by the two state scaled model. The solid line shows the result of model sum. The line shows raw data. (D) The fitting data of FliG constructs. The solid lines show the result of model sum for full length $FliG_{Full}$, G122-$FliG_{MC}$, and G214-$FliG_C$.

prevents the effects of electrostatic charge.

In the CD spectroscopic analysis, the constructs showed differences in their negative peaks between the two pH conditions (Fig. 3). All spectra at pH 6.5 showed higher negative peaks than those at pH 8.0. These results suggest that the structures under pH 6.5 seem to contain more secondary structures than those under pH 8.0. Furthermore, in *Salmonella*, it was reported that the CD spectra of $FliG_C$ does not change under broad temperature conditions (15–45°C) [30], suggesting that temperature may not severely affect the structure of FliG compared to pH. As discussed above, at pH 6.5 FliG exists in its compact form, leading to the conclusion that the compact form of FliG has more secondary structures and the electrostatic interactions may have an important role for this conformation of FliG.

We measured the thermal stability of FliG constructs using DSC. In $FliG_C$, one peak appeared in the profile and the T_m value was ca. 60°C (Fig. 4A). This value is reasonable because CD spectroscopic analysis revealed that $FliG_C$ does not change its secondary structure until 45°C [30]. In the case of $FliG_{Full}$ and $FliG_{MC}$, there were several peaks in the profiles but the number of peaks corresponded with the number of domains of the constructs (Fig. 4B, C). Therefore, we propose that each domain of FliG independently denatures. Moreover, it is difficult to assign each domain a T_m value because there are various T_m values for the FliG constructs. This indicates that the interactions between domains also have some roles in thermal stability.

In summary, this study may support the recent report showing that in solution, FliG from *E. coli* has two conformations: an extended form and a compact form [29]. Here, using FliG from *Vibrio* we demonstrated that these conformations might be regulated by controlling pH conditions, suggesting an important role of electrostatic charges in the structural conformation of FliG. These findings implicate that the two conformations might be related to the state of the two rotational directions, CCW and CW, and these conformations are conserved among bacterial species. In the bacterial cell, it has been suggested that FliG forms a domain-swapped polymer when it assembles in the flagellar motor [20,29]. Therefore, it is essential to explore the mechanism of assembly for forming ring-like structures in the flagellar motor and the biophysical properties of FliG clarified in this study will assist to clarify the mechanism.

Acknowledgments

This study was funded by grants-in-aid for scientific research from the Ministry of Education, Science and Culture of Japan (24117004 and 23247024 to MH), and the Program for leading Graduate Schools of Japan Science for the Promotion of Science to MG and YN.

Conflict of Interest

The authors declare that they have no conflict of interest.

Author Contributions

Y. O., Y. N., R. A.-Y., and M.H. designed experiments. R. A.-Y., M. G., and S. K. performed experiments. Y. N., R. A.-Y., Y. O., Y. A., and M. H. analyzed the data. Y. N., Y. O., and M. H. wrote the manuscript. M. H. supervised the study.

References

[1] Zhou, J., Lloyd, S. A. & Blair, D. F. Electrostatic interactions between rotor and stator in the bacterial flagellar motor. *Proc. Natl. Acad. Sci. USA* **95**, 6436–6441 (1998).
[2] Takekawa, N., Kojima, S. & Homma, M. (2014) Contribution of many charged residues at the stator-rotor interface of the Na^+-driven flagellar motor to torque generation in *Vibrio alginolyticus*. *J. Bacteriol.* **196**, 1377–1385.
[3] Yorimitsu, T. & Homma, M. Na^+-driven flagellar motor of *Vibrio*. *Biochim. Biophys. Acta* **1505**, 82–93 (2001).
[4] Blair, D. F. Flagellar movement driven by proton translocation. *FEBS Lett.* **545**, 86–95 (2003).
[5] Sato, K. & Homma, M. Multimeric structure of PomA, a component of the Na^+-driven polar flagellar motor of *Vibrio alginolyticus*. *J. Biol. Chem.* **275**, 20223–20228 (2000).
[6] Kojima, S. & Blair, D. F. Solubilization and purification of the MotA/MotB complex of *Escherichia coli*. *Biochemistry* **43**, 26–34 (2004).
[7] Kojima, S., Imada, K., Sakuma, M., Sudo, Y., Kojima, C., Minamino, T., *et al.* Stator assembly and activation mechanism of the flagellar motor by the periplasmic region of MotB. *Mol. Microbiol.* **73**, 710–718 (2009).
[8] Zhu, S., Takao, M., Li, N., Sakuma, M., Nishino, Y., Homma, M., *et al.* Conformational change in the periplamic region of the flagellar stator coupled with the assembly around the rotor. *Proc. Natl. Acad. Sci. USA* **111**, 13523–13528 (2014).
[9] Parkinson, J. S. & Kofoid, E. C. Communication modules in bacterial signaling proteins. *Annu. Rev. Genet.* **26**, 71–112 (1992).
[10] Francis, N. R., Sosinsky, G. E., Thomas, D. & Derosier, D. J. Isolation, characterization and structure of bacterial flagellar motors containing the switch complex. *J. Mol. Biol.* **235**, 1261–1270 (1994).
[11] Toker, A. S. & Macnab, R. M. Distinct regions of bacterial flagellar switch protein FliM interact with FliG, FliN and CheY. *J. Mol. Biol.* **273**, 623–634 (1997).
[12] Levenson, R., Zhou, H. & Dahlquist, F. W. Structural insights into the interaction between the bacterial flagellar motor proteins FliF and FliG. *Biochemistry* **51**, 5052–5060 (2012).
[13] Welch, M., Oosawa, K., Aizawa, S. I. & Eisenbach, M. Phosphorylation-dependent binding of a signal molecule to the flagellar switch of bacteria. *Proc. Natl. Acad. Sci. USA* **90**, 8787–8791 (1993).
[14] Welch, M., Oosawa, K., Aizawa, S. I. & Eisenbach, M. Effects of phosphorylation, $Mg2^+$, and conformation of the chemotaxis protein CheY on its binding to the flagellar switch protein FliM. *Biochemistry* **33**, 10470–10476 (1994).
[15] Brown, P. N., Hill, C. P. & Blair, D. F. Crystal structure of the middle and C-terminal domains of the flagellar rotor protein FliG. *EMBO J.* **21**, 3225–3234 (2002).
[16] Lee, L. K., Ginsburg, M. A., Crovace, C., Donohoe, M. &

Stock, D. Structure of the torque ring of the flagellar motor and the molecular basis for rotational switching. *Nature* **466**, 996–1000 (2010).
[17] Minamino, T., Imada, K., Kinoshita, M., Nakamura, S., Morimoto, Y. V. & Namba, K. Structural insight into the rotational switching mechanism of the bacterial flagellar motor. *PLoS Biol.* **9**, e1000616 (2011).
[18] Vartanian, A. S., Paz, A., Fortgang, E. A., Abramson, J. & Dahlquist, F. W. Structure of flagellar motor proteins in complex allows for insights into motor structure and switching. *J. Biol. Chem.* **287**, 35779–35783 (2012).
[19] Lam, K. H., Ip, W. S., Lam, Y. W., Chan, S. O., Ling, T. K. & Au, S. W. Multiple conformations of the FliG C-terminal domain provide insight into flagellar motor switching. *Structure* **20**, 315–325 (2012).
[20] Sircar, R., Borbat, P. P., Lynch, M. J., Bhatnagar, J., Beyersdorf, M. S., Halkides, C. J., *et al.* Assembly states of FliM and FliG within the flagellar switch complex. *J. Mol. Biol.* **427**, 867–886 (2015).
[21] Dyer, C. M., Vartanian, A. S., Zhou, H. & Dahlquist, F. W. A molecular mechanism of bacterial flagellar motor switching. *J. Mol. Biol.* **388**, 71–84 (2009).
[22] Lloyd, S. A., Tang, H., Wang, X., Billings, S. & Blair, D. F. Torque generation in the flagellar motor of *Escherichia coli*: evidence of a direct role for FliG but not for FliM or FliN. *J. Bacteriol.* **178**, 223–231 (1996).
[23] Yorimitsu, T., Mimaki, A., Yakushi, T. & Homma, M. The conserved charged residues of the C-terminal region of FliG, a rotor component of the Na^+-driven flagellar motor. *J. Mol. Biol.* **334**, 567–583 (2003).
[24] Yorimitsu, T., Sowa, Y., Ishijima, A., Yakushi, T. & Homma, M. The systematic substitutions around the conserved charged residues of the cytoplasmic loop of Na^+-driven flagellar motor component PomA. *J. Mol. Biol.* **320**, 403–413 (2002).
[25] Yakushi, T., Yang, J., Fukuoka, H., Homma, M. & Blair, D. F. Roles of charged residues of rotor and stator in flagellar rotation: comparative study using H^+-driven and Na^+-driven motors in *Escherichia coli*. *J. Bacteriol.* **188**, 1466–1472 (2006).
[26] Onoue, Y., Kojima, S. & Homma, M. Effect of FliG three amino acids deletion in *Vibrio* polar-flagellar rotation and formation. *J. Biochem. (Tokyo)* **158**, 523–529 (2015).
[27] Kojima, S., Nonoyama, N., Takekawa, N., Fukuoka, H. & Homma, M. Mutations targeting the C-terminal domain of FliG can disrupt motor assembly in the Na^+-driven flagella of *Vibrio alginolyticus*. *J. Mol. Biol.* **414**, 62–74 (2011).
[28] Gohara, M., Kobayashi, S., Abe-Yoshizumi, R., Nonoyama, N., Kojima, S., Asami, Y. & Homma, M. Biophysical characterization of the C-terminal region of FliG, an essential rotor component of the Na^+-driven flagellar motor. *J. Biochem. (Tokyo)* **155**, 83–89 (2014).
[29] Baker, M. A., Hynson, R. M., Ganuelas, L. A., Mohammadi, N. S., Liew, C. W., Rey, A. A., *et al.* Domain-swap polymerization drives the self-assembly of the bacterial flagellar motor. *Nat. Struct. Mol. Biol.* **23**, 197–203 (2016).
[30] Hashimoto, M., Momma, K., Inaba, S., Nakano, S. & Aizawa, S. The hydrophobic core of FliG domain II is the stabilizer in the *Salmonella* flagellar motor. *Microbiology* **158**, 2556–2567 (2012).
[31] Ogawa, R., Abe-Yoshizumi, R., Kishi, T., Homma, M. & Kojima, S. Interaction of the C-Terminal tail of FliF with FliG from the Na^+-driven flagellar motor of *Vibrio alginolyticus*. *J. Bacteriol.* **197**, 63–72 (2015).